STORM-INDUCED VARIABILITY OF LONGSHORE SEDIMENT TRANSPORT IN BOU-ISMAIL BAY, ALGERIA

Abd El Alim DAHMANI*[1,4], Yousra SALEM-CHERIF[1,4], Miloud SALLAYE[2,4], Redouane BOURKACHE[3], Sidahmed BENZERFA[1], Khoudir MEZOUAR[1,4]

[1]National Higher School of Marine Science and Coastal Development (ENSSMAL), Dely Ibrahim, Algiers, Algeria
e-mail: yousra.salem-cherif@enssmal.edu.dz; sidahmedbenzerfa@gmail.com; khoudir.mezouar@enssmal.edu.dz
[2]Department of Earth Sciences, Institute of Architecture and Earth Sciences, University Ferhat Abbas, Setif 1, Algeria
e-mail: sallaye.miloud@gmail.com
[3]Maritime Studies Laboratory (LEM), Bp 848, Djenane El Malik. Hydra, Algiers, Algeria
e-mail: redouane.bourkache@lem-dz.com
[4]ENSSMAL - Laboratory of Marine and Coastal Ecosystems (ECOSYSMarL), Dely Ibrahim, Algiers, Algeria
**Corresponding author: abdelalim.dahmani@enssmal.edu.dz; https://orcid.org/0009-0009-4020-9830*

DOI: 10.5281/zenodo.17938993

Abstract. This study investigates the longshore sediment transport (LST) dynamics under extreme wave conditions along Bou-Ismail Bay, Algeria. A hindcast dataset covering 29 years (1992-2020) was analysed using a POT (Peak Over Threshold) extreme value approach, combined with DHI MIKE 21 spectral wave modelling to simulate wave transformation from offshore to nearshore. LST rates were then quantified using the recalibrated formulation of Mil-Homens *et al.* (2013). The results indicate that LST responds non-linearly to storms. An increase of only 1 to 2 m in significant wave height (H_s) was sufficient to multiply transport rates, highlighting the crucial role of extreme conditions relative to mild wave conditions. The Sidi Fredj headland proved to be a dominant geomorphological factor, protecting *Khelloufi* beach from northeast swells while exposing *Colonel Abbas* to the direct action of northern and western waves. Morphodynamic contrasts further explain the differences observed in the LST. The steeper breaking zone at *Colonel Abbas* (slope of 0.09) increased wave height, while the finer sands (260 µm) were more mobile than those at *Khelloufi*, where the slope is gentler (0.03) and the sediments coarser (330 µm). The integrated methodology proved to be robust and reliable revealing that extreme-event-driven LST must be incorporated into sediment budgets, risk assessments, and shoreline management for effective and sustainable coastal planning.

Key words: Longshore sediment transport (LST), Peak Over Threshold (POT), Morphodynamic, Extreme wave, Bou-Ismail Bay

1. INTRODUCTION

The shoreline constitutes one of the most significant linear features on earth, making beach management a constant concern for nearly all coastal regions (Sallaye *et al.*, 2022; Shaeri *et al.*, 2020). Among the processes that control coastal morphology, longshore drift (or LST), expressed as average transport rates over extended time scales, plays a major role (Bird, 2008; CERC, 1984; Komar, 1998; Kuriyama and Sakamoto, 2014).

Calculation of LST rate is involved in a number of engineering and beach management problems, such as the description of beach dynamics, the reliability assessment of a coastal structure, or the investigation of wave-beach-structure interaction (Arena *et al.*, 2013; Barbaro *et al.*, 2014; Dahmani *et al.*, 2021; Tomasicchio *et al.*, 2011).

LST is mainly driven by longshore currents generated due to the cross-shore gradient in the alongshore shear component of the radiation stress, which is in turn driven by obliquely incident breaking waves (Longuet-Higgins, 1970). Due to this large dependence of the longshore current on breaking wave properties (Mackay *et al.*, 2010), most widely

used LST equations are based on surf zone properties (Mil-Homens *et al.*, 2013).

Numerous formulas and models have been proposed to calculate LST rates, evolving from early fundamental work to increasingly complex parameterizations. This field was pioneered by Munch-Peterson (1938), with significant empirical contributions from Saville (1950) and Caldwell (1967). The theoretical foundations were established by Inman and Bagnold (1963), leading to the ubiquitous CERC formula, as formalized in the Shore Protection Manual (CERC, 1984). This formula was followed by noteworthy contributions from Bijker (1971), who integrated wave-current interactions, and Bailard (1982), who developed Bagnold's energy model. The end of the 20th century saw the development of physics-based formulas by Kamphuis (1991) and global approaches by Van Rijn (1993). The last few decades have been marked by improvements such as the energy flux approach of Bayram *et al.* (2007), large-scale recalibrations by Mil-Homens *et al.* (2013), the spectral effect (Barbaro *et al.*, 2014) and the D_{50} influence (Van Rijn, 2014).

These formulas incorporate a wide range of morphological and hydrodynamic parameters, and their accuracy can be significantly improved by the valuable contribution of numerical modelling of key variables (Jiang *et al.*, 2011; Shanas and Sanil Kumar, 2014).

While several studies conducted along the Algerian coast have employed bulk formulas to estimate the LST under moderate wave conditions (Salem Cherif *et al.*, 2019), the impact of extreme weather and sea events (*e.g.*, storms, storm surges) on these dynamics remains largely unexplored. Filling this critical knowledge gap is one of the main motivations for this research. A thorough understanding of these interactions and process related to extreme events is fundamental to implementing sustainable and effective coastal management strategies that ensure both economic stability and environmental resilience.

2. STUDY AREA

Bou-Ismail Bay, is a significant embayment located on Algeria's central Mediterranean coast, approximately 45 km west of the capital, Algiers. The bay stretches from the Sidi Fredj headland in the east to the tip of the Chenoua Plateau in the west, forming a wide, open arc roughly 40 km wide (Fig. 1). Geomorphologically and hydrologically, the bay is characterized by a diverse coastal morphology, including sandy beaches, an alluvial plain, and a river mouth backed by the coastal hills of the Tell Atlas range, which descend sharply into the sea, creating a narrow continental shelf.

Its strategic location in the wilaya (province) of Tipaza places it in a region of high economic and recreational importance, supporting key infrastructure including commercial and numerous fishing harbours and known by its high tourism potential and recreation area.

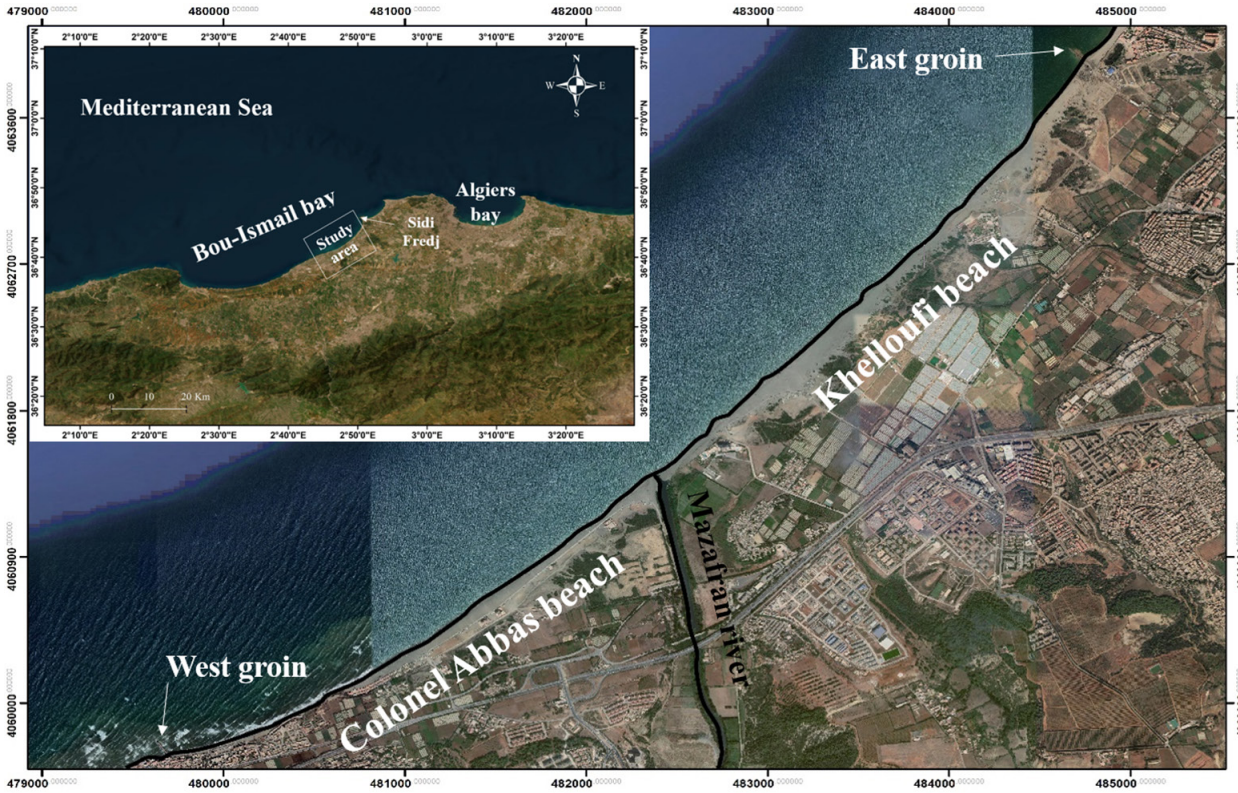

Fig. 1. Physiographic context and location of the study area.

The selected study area comprises two adjacent beaches located in different administrative provinces: *Khelloufi* beach in Algiers and *Colonel Abbas* beach in Tipaza. These sites are naturally separated by the Mazafran River, which is the main source of sediment input for the entire Bou-Ismail Bay. The coastal unit studied is bounded laterally by two groins (Fig. 1), positioned eastward and westward, which act as structural boundaries for the coastal cell.

3. WIND WAVE CLIMATOLOGY AND TIDE

The wave climate of the study area, which encompasses both offshore and nearshore hydrodynamics and extreme event analysis, was characterized using a 29 year hindcast (1992-2020) for a location in deep water (36.75°N, 2.5°E) (INFOPLAZA, 2021). The dataset, sourced from www.waveclimate.com, includes spectral parameters for locally generated wind waves and swells originating from the northern Mediterranean.

Statistical analysis of offshore wave directions enabled us to construct seasonal wave roses (Fig. 2). These indicate that the dominant waves come from the northeast, accounting for 24% of annual occurrences, with higher frequencies in summer (42%), spring (33%), and winter (15.1%) than in autumn (13%). Western waves account for 11% of annual occurrences, with higher frequencies in spring (15.6%), autumn (13.2%), and winter (10%) compared to summer (6%).

It should be noted that the highest waves (H_s > 5 m), although infrequent, were mainly generated by winter storms from the west and northeast. In addition, the analysis revealed that approximately 58% of the recorded waves from all directions were less than one meter high.

4. DATA AND METHODOLOGY

4.1. Extreme value analysis

In this study, the POT (Peak Over Threshold) method was applied to wave height data and then fitted using a generalized Pareto distribution (GPD) (Vinoth and Young, 2011). This approach was chosen because it offers significant advantages over the traditional annual maximum method, in that it incorporates all wave events exceeding a predefined threshold rather than limiting the analysis to the highest value for each year (Coles, 2001). As a result, it also captures the second, third, or even fourth peaks in a year, some of which may exceed the maxima of other years (Guedes Soares and Scotto, 2004). This feature makes the method particularly suitable for relatively short time series (Grandry *et al.*, 2018).

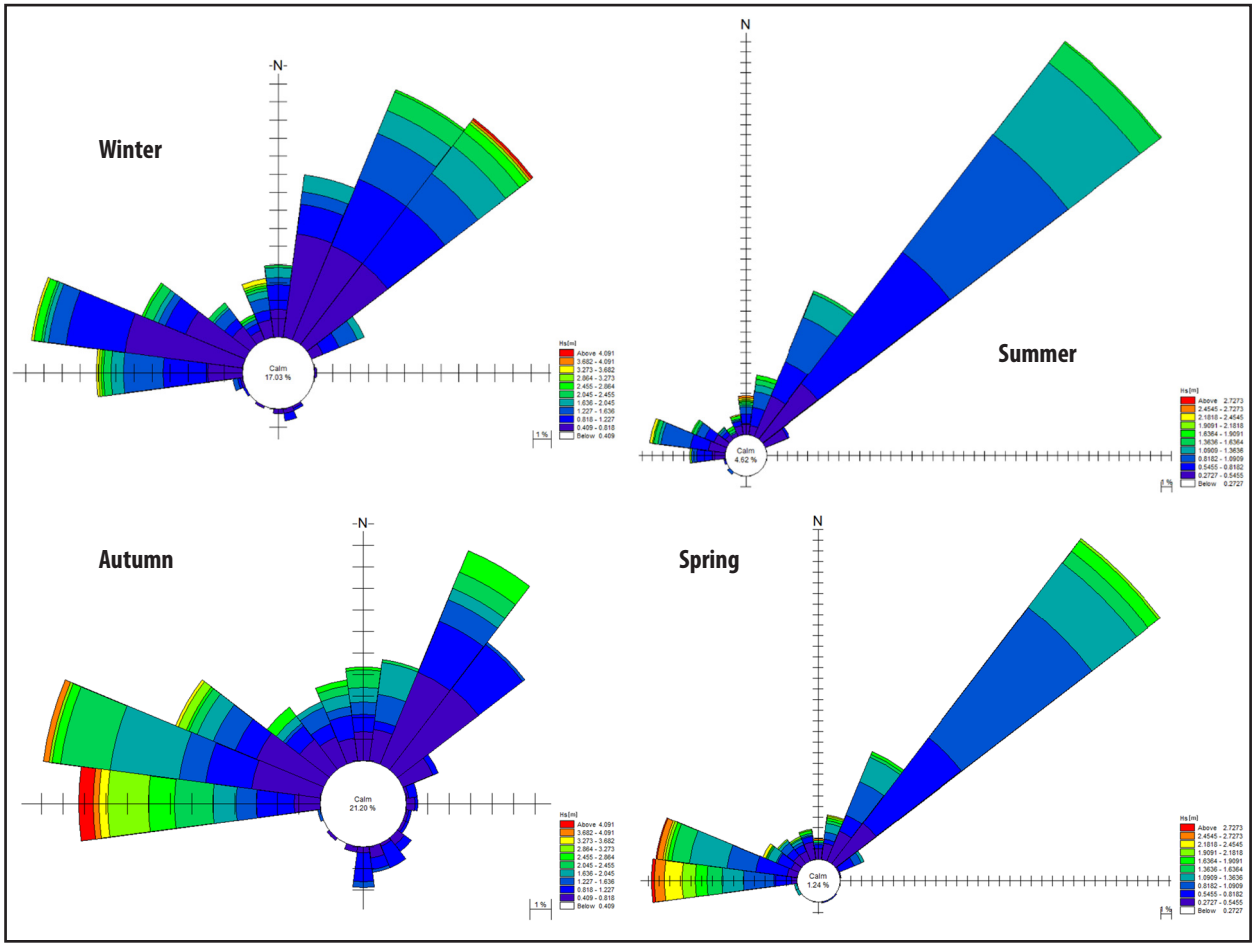

Fig. 2. Seasonal wave diagrams derived from the INFOPLAZA (2021) database (1992-2020).

Nevertheless, extracting POT events is known to be methodologically challenging and time-consuming. The most critical step is determining the threshold, which must be set low enough to ensure a sufficient number of exceedances, while remaining high enough to ensure the statistical independence of the selected peaks. Among the various techniques and rules of thumb available in the literature for selecting thresholds, this study adopted the 97th percentile, corresponding to approximately 3 m (Alves and Young, 2003; Caires and Sterl, 2005; Challenor *et al.*, 2005; Salcedo-Castro *et al.*, 2018).

4.2. Mike 21 Numerical model

The wave transformation simulation, from the offshore to the nearshore, was performed using the MIKE 21 Spectral Waves (SW) model developed by DHI (2017). This tool was used to determine critical wave parameters, including significant wave height (H_s), peak period (T_p), and mean direction (°).

MIKE 21 SW is a sophisticated spectral model that accounts for the generation, propagation, and transformation of wind waves and swell. It is widely used in coastal engineering, providing robust and reliable simulations that are essential for infrastructure design, environmental assessments, and coastal risk management (DHI, 2017).

For large-scale wave propagation simulations, *the fully spectral formulation* combined with *the in-stationary formulation* was configured as the governing equations. The initial wave spectra were defined according to the JONSWAP parameterization, widely recognized for representing sea states limited by fetch length. In order to correctly capture directional variability, four main wave approach angles were imposed: north (0°), northeast (45°), west (270°), and northwest (315°). For each direction, simulations were performed under three distinct significant wave height (H_s) conditions, corresponding to return periods of 1, 10, and 100 years (Table 1).

4.3. Bathymetric data

The bathymetric data used in this study was derived from two complementary sources. Offshore depths greater than 10 m were extracted from the Navionics digital database (www.navionics.com), while shallow water bathymetry (0 to 10 m) was obtained through a dedicated reconnaissance survey.

The bathymetric surface obtained was represented using an unstructured triangular mesh, which allowed for variable spatial resolution (Fig. 3). A high level of accuracy was applied in the coastal area in order to accurately capture the coastal morphology, with a gradual transition to an intermediate resolution at mid-depth and coarser elements beyond the closure depth.

Sediment characterization of the study area revealed a predominance of medium sands, the median grain size ranging from 260 µm at *Colonel Abbas* beach to 330 µm at *Khelloufi* beach, reflecting the spatial variability of the coastal granulometric composition.

4.4. Longshore sediment transport formulae

The Mil-Homens et al. (2013) formulae

Since no single formula has been universally recommended for assessing LST, we selected the Mil-Homens *et al.* (2013) formulae for application in this study. This formulation benefits extensively from a reassessment of

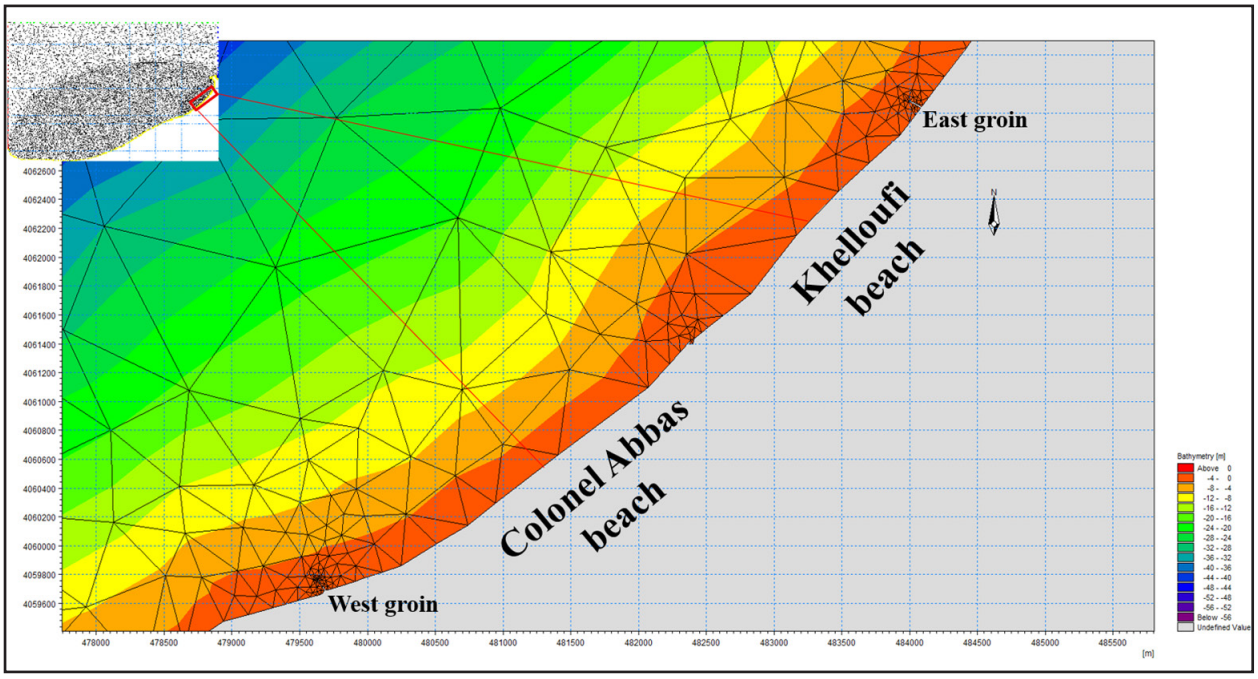

Fig. 3. Triangular mesh of Bou-Ismail Bay (upper left) with corresponding bathymetric map of the study area.

previous empirical approaches, notably the Kamphuis (1991) equation, with recalibrated coefficients that account for several key parameters influencing LST (Equation 1).

Mil-Homens *et al.* (2013) validated their modifications using a reliable dataset comprising approximately 250 experimental and field observations, widely representative of sandy beaches, thus providing a more reliable prediction tool (see also Van Rijn, 2014).

$$Q = k_{MH,KPH} H_{sb}^{2.75} T_P^{0.98} m_b^{0.86} D_{50}^{-0.69} sin^{0.5}(2\alpha_b) \quad (1)$$

where:

$$k_{MH,KPH} = \frac{0.149}{(\rho_s - \rho)(1-p)}$$

Q = sediment transport rate (m^3/s).

H_{sb} = significant wave height at the breaking point (m)

T_P = peak period (s)

m_b = bottom slope in the surf zone

D_{50} = sediment grain size (m)

α_b = angle between wave crest and shoreline at breaking line (°)

p = porosity (p = 0.4)

ρ_s = sediment density (kg/m^3)

ρ = water density (kg/m^3)

5. RESULTS AND DISCUSSIONS

5.1. Extreme wave height values

Drawing on the treatments and the analysis of the INFOPLAZA (2021) databases, (Fig. 4) and (Table 1) summarize the threshold value (3 m) and all return level results for several return periods.

As might be expected, the variability of the estimates is higher for the 10- and 100-year return periods than for the 1-year return periods, since these are extrapolations.

The obtained results from the database analysis, in particular the estimated return values, provide strong evidence for the reliability of the POT method for characterizing extreme waves. The computed 30-year significant wave height of 6.56 m (Table 1) corresponds remarkably well with the highest offshore measurement (6.85 m) over a 29-year survey period, reinforcing confidence in the methodology and predictive capability of the model for long-term coastal engineering applications.

5.2. Numerical modelling results

The influence of the four prevailing wave directions on the Bou-Ismail shoreline is highly variable.

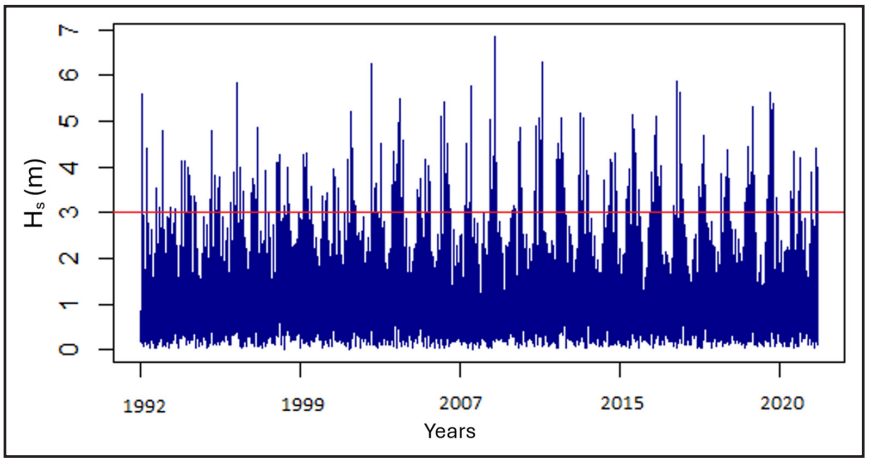

Fig. 4. Significant wave height time series derived from the POT approach (threshold: 3 m).

Table 1. Return levels of significant wave height for the overall dataset.

Return period (years)	Return value (H_s) (m)
1	4.74
5	5.71
10	6.06
20	6.38
30	6.56
50	6.77
100	7.03

Figure 5 shows that, in the case of 1-yr wave height, offshore gravity waves undergo systematic energy dissipation as they approach the coast.

Refraction dominates for waves approaching from 270° (W) and 315° (NW), while diffraction clearly controls the propagation of waves from 45° (NE) and, to a lesser extent, 0° (N) around Cape Sidi Fredj.

For all the extreme wave return periods considered, the results consistently show that *Colonel Abbas* beach is subject to significantly higher wave heights than *Khelloufi* beach. This difference is governed by local morphodynamic conditions, as the steep foreshore gradient (slope of the nearshore seabed) of the *Colonel Abbas* beach favours wave shoaling compared to the gentler slope at *Khelloufi* beach.

5.3. Longshore sediment transport

The comparative results of the LST in Bou-Ismail Bay for the two investigated sites, *Khelloufi* and *Colonel Abbas* beaches, obtained using the Mil-Homens (2013) formula for the four wave directions aforementioned and under three extreme wave scenarios (1-year, 10-year, and 100-year return periods), are presented in tables 2 and 3 and figures 6 and 7.

As expected, for the two beaches and all wave directions considered, the LST rates associated with the 100-year return period are higher than those corresponding to the 10-year scenario, which in turn exceed the values obtained under annual wave conditions. This trend is mainly attributed to the gradual increase in the significant height of breaking waves (H_{sb}) between annual, decadal, and centennial events, which constitutes a key control variable in Mil-Homens *et al.* (2013) formulation.

5.3.1. Khelloufi beach

The results clearly indicate the predominance of the NE (45°) direction over other orientations, with an associated LST rate of 0.00729 m^3/s under annual wave conditions, compared to 0.00364, 0.00418, and 0.00474 m^3/s for the N (0°), NW (315°), and W (270°) directions, respectively.

It is also clear that the rates associated with these last three directions tend to converge under annual conditions, reaching 0.00284, 0.00280, and 0.00308 m^3/s, correspondingly.

This behaviour can be largely attributed to the higher wave incidence angle associated with the NE sector, which is strongly influenced by the coastal headland, reinforcing wave refraction towards the shore and thus promoting more efficient sediment transport through stronger longshore currents.

5.3.2. Colonel Abbas beach

For this beach, the LST rate associated with the N direction (0°) is clearly dominant compared to the other orientations, reaching 0.0532 m^3/s in decadal wave conditions, compared to 0.0273, 0.0134, and 0.0295 m^3/s for the NE (45°), NW (315°) and W (270°) directions, respectively.

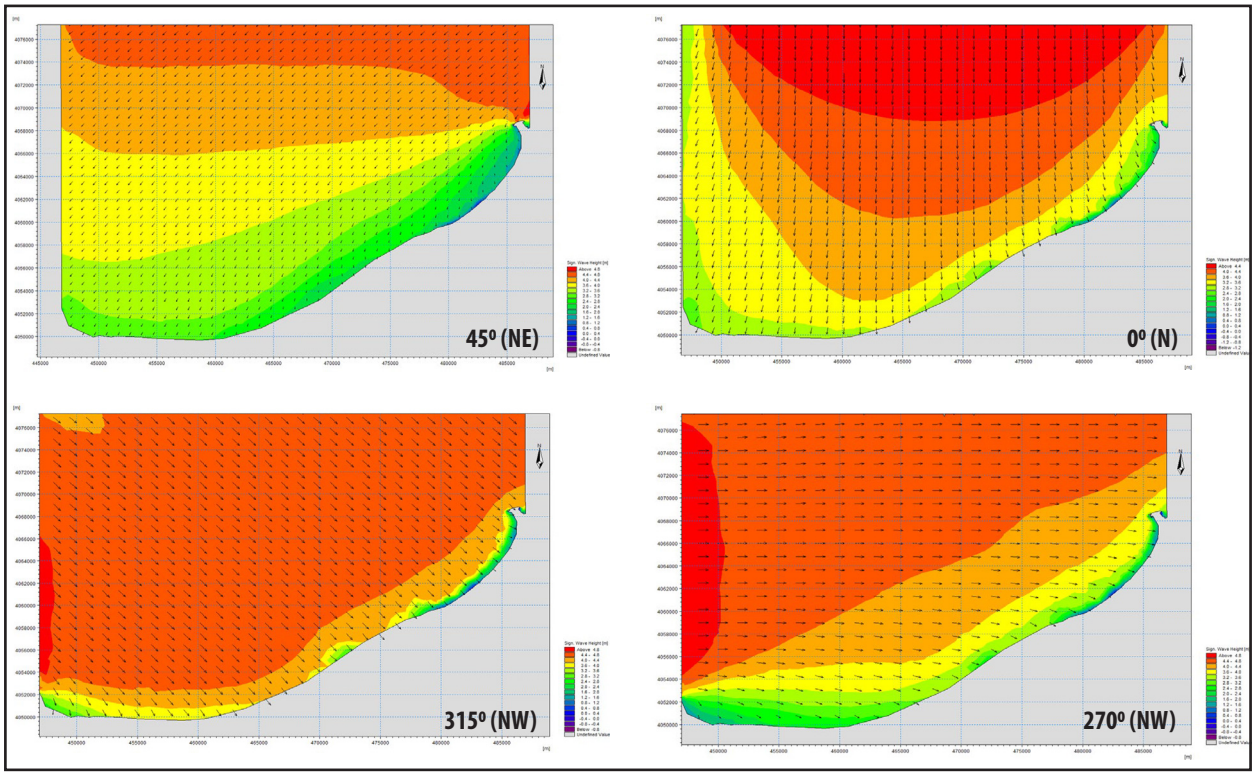

Fig. 5. Spatial distribution of significant wave heights under 1-year return level.

Table 2. Longshore sediment transport rate at *Khelloufi* beach (m^3/s).

	NE (45°)	N (0°)	NW (315°)	W (270°)
Annual	0.00496	0.00284	0.0028	0.00308
Decadal	0.00729	0.00364	0.00418	0.00474
Centennial	0.0108	0.00439	0.00577	0.00671

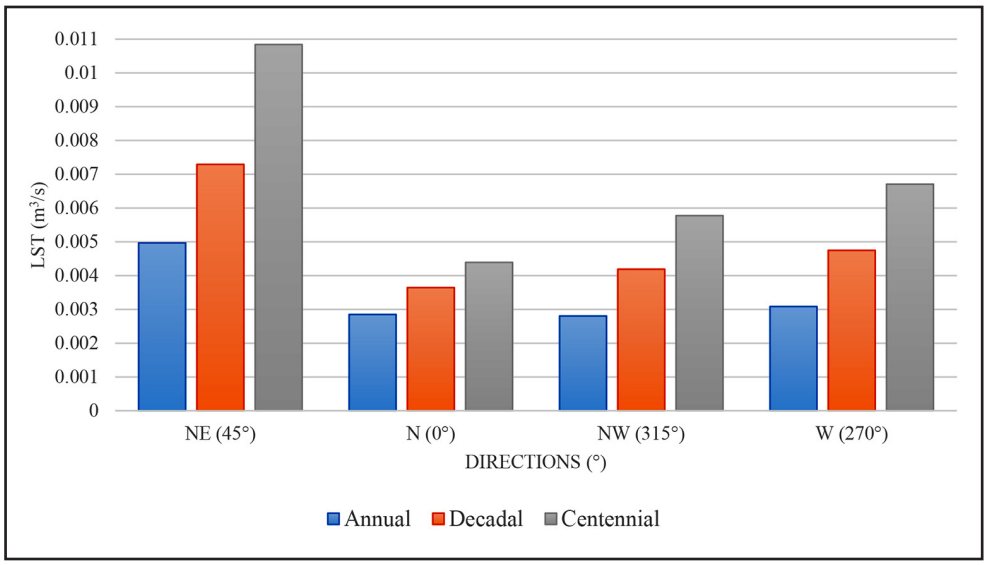

Fig. 6. Histogram representation of longshore sediment transport rates at *Khelloufi* beach (m^3/s).

Table 3. Longshore sediment transport rate at *Colonel Abbas* beach (m^3/s).

	NE (45°)	N (0°)	NW (315°)	W (270°)
Annual	0.0203	0.0325	0.0101	0.0213
Decadal	0.0273	0.0532	0.0134	0.0295
Centennial	0.0327	0.0626	0.0173	0.0498

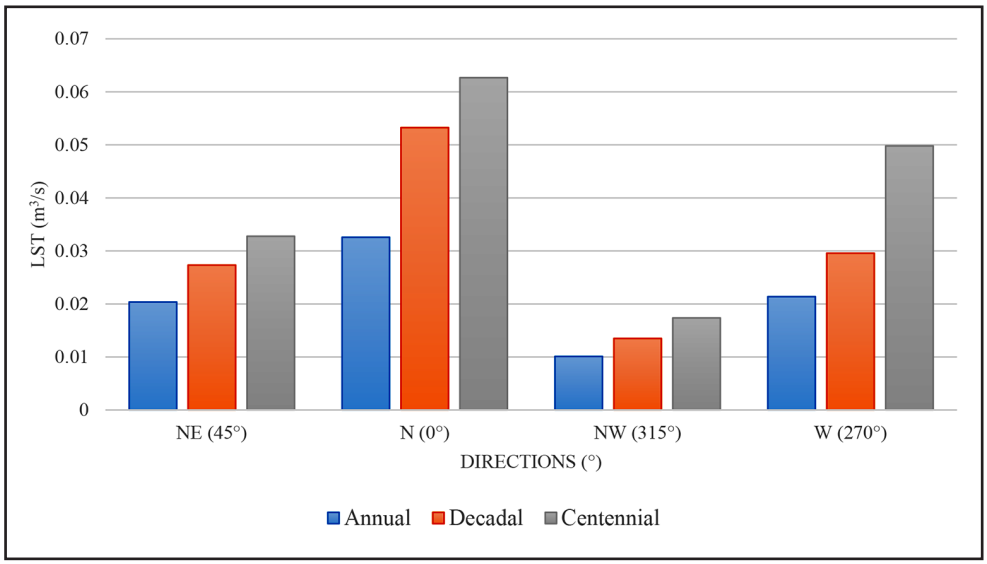

Fig. 7. Histogram representation of longshore sediment transport rates at *Colonel Abbas* beach (m^3/s).

It should be noted that an exception occurs for centennial waves, where the transport rates for W (270°) and N (0°) converge, with values of 0.0498 and 0.0626 m^3/s.

These findings can largely be explained by the geomorphological configuration of the site, which is oriented SW-NE and lies directly in the lee of the Sidi Fredj headland. As a result, the beach is well protected from NE waves (45°), while waves from the N sector (0°) can still generate high angles of incidence and strong longshore currents, resulting in high LST rates.

A comparative analysis of LST rates between the two beaches reveals significantly higher transport values at *Colonel Abbas* than at *Khelloufi*. This phenomenon can be explained largely by morphodynamic differences: the slope of the surf zone at *Colonel Abbas* (0.09) is three times steeper than at *Khelloufi* (0.03), resulting in deeper break points and increased surf height nearshore. As a result, a greater flow of wave energy is available to drive longshore currents and sediment transport. In addition, sediment characteristics exert a secondary influence, as the finer median grain size (D_{50} = 260 µm) at *Colonel Abbas* is more easily mobilized than the coarser material at *Khelloufi* (D_{50} = 330 µm).

6. CONCLUSIONS

This study's results clearly show the nonlinear sensitivity of LST to extreme waves. An increase of only 1 to 2 m in significant wave height (H_s) led to multiply LST rates by a factor of two or more. This highlights the critical role of extreme events in sediment transport and coastal reshaping, well beyond moderate and mild hydrodynamic conditions.

The Sidi Fredj headland proved to be a key geomorphological factor, modulating wave propagation patterns in Bou-Ismail Bay. By protecting *Khelloufi* Beach from northeast swells while exposing *Colonel Abbas* to north and west waves, it introduced marked contrasts in LST amplitude and direction.

Local morphodynamic and sediment properties also played a decisive role. The steeper breaking zone at *Colonel Abbas* (slope ≈ 0.09) resulted in deeper breaking conditions and greater breaking heights, thereby increasing transport potential. This effect was reinforced by the finer median size of the sediments (260 µm), which are more easily mobilized than the coarser grains at *Khelloufi* (330 µm). Wave incidence angles further amplified these variations.

The integration of POT (Peak Over Threshold) statistics, MIKE21 wave spectral model simulations and the Mil-Homens *et al.* (2013) formula proved to be robust. In practical terms, these results highlight the need to integrate LST related to extreme events into sediment budgets and coastal management plans. For Bou-Ismail Bay and similar Mediterranean coasts, coastal infrastructure design and adaptation strategies must explicitly take into account storm-induced LST and headland-induced gradients.

AUTHOR CONTRIBUTION

Abd El Alim Dahmani: Formal analysis, Conceptualization, Methodology, Investigation, Visualization, Writing - original draft. **Miloud Sallaye**: Data curation, Visualization, Writing - review and editing. **Yousra Salem Cherif**: Methodology, Resources, Writing - review and editing. **Redouane Bourkache**: Investigation, Writing - review and editing. **Sidahmed Benzerfa**: Investigation, Writing - review and editing. **Khoudir Mezouar**: Formal analysis, Conceptualization, Writing – review and editing.

REFERENCES

Alves, J.H.G.M., Young, I.R. (2003). On estimating extreme wave heights using combined Geosat, Topex/Poseidon and ERS-1 altimeter data. *Appl. Ocean Res.*, **25**(*4*): 167–186. https://doi.org/10.1016/J.APOR.2004.01.002

Arena, F., Laface, V., Barbaro, G., Romolo, A. (2013). Effects of Sampling between Data of Significant Wave Height for Intensity and Duration of Severe Sea Storms. *Int. J. Geosci.*, **4**(*1A*): 240–248. https://doi.org/10.4236/IJG.2013.41A021

Bailard, J.A. (1982). An energetics total load sediment transport model for a plane sloping beach. Final technical note Oct 80-Sep 81, NAVAL CIVIL ENGINEERING LAB PORT HUENEME CA, 69 p. URL https://apps.dtic.mil/sti/citations/ADA116588

Barbaro, G., Foti, G., Sicilia, L., Malara, G. (2014). A formula for the calculation of the longshore sediment transport including spectral effects. *J. Coast. Res.*, **30**(*5*): 961–966. https://doi.org/10.2112/JCOASTRES-D-13-00131.1

Bayram, A., Larson, M., Hanson, H. (2007). A new formula for the total longshore sediment transport rate. *Coast. Eng.*, **54**(*9*): 700–710. https://doi.org/10.1016/J.COASTALENG.2007.04.001

Bijker, E. (1971). Longshore transport computations. ASCE - *J. Waterw. Harb. Coast. Eng. Div.*, **97**(*4*): 687–701. doi:10.1061/AWHCAR.0000122

Bird, E. (2008). Coastal Geomorphology: an introduction - Second Edition, John Wiley & Sons Ltd, The Atrium, Southern Gate, Chichester, 436 p.

Caires, S., Sterl, A. (2005). 100-Year Return Value Estimates for Ocean Wind Speed and Significant Wave Height from the ERA-40 Data. *J. Clim.*, **18**: 1032–1048. https://doi.org/10.1175/JCLI-3312.1

Caldwell, J. (1967). Coastal processes and beach erosion. U.S. Army Coastal Engineering Research Center.

CERC (1984). Shore protection manual. Coastal Engr. Res. Center, U.S. Army Corps of Engrs. Washington, D.C.

Challenor, P.G., Wimmer, W., Ashton, I. (2005). Climate change and extreme wave heights in the North Atlantic. In: *Proc. of the 2004 Envisat & ERS Symposium*, Salzburg, Austria 6-10 September 2004 (ESA SP-572, April 2005), *Eur. Sp. Agency, Special Publ.* (ESA SP): 1253–1257.

Coles, S. (2001). An introduction to statistical modeling of extreme values. Springer Series in Statistics, Springer-Verlag London, 208 p. https://doi.org/10.1007/978-1-4471-3675-0

Dahmani, A. El Alim, Mezouar, K., Salem Cherif, Y., Sallaye, M. (2021). Coastal processes and nearshore hydrodynamics under high contrast wave exposure, Bateau-cassé and Stamboul coasts, Algiers Bay. *Estuar. Coast. Shelf Sci.*, **250**, 107169. https://doi.org/10.1016/j.ecss.2021.107169

DHI (2017). MIKE 21 Documentation. http://manuals.mikepoweredbydhi.help/2017/MIKE_21.htm

Grandry, M., Degré, A., Gailliez, S. (2018). HydroTrend - Rapport final. https://doi.org/10.3/JQUERY-UI.JS

Guedes Soares, C., Scotto, M.G. (2004). Application of the **r** largest-order statistics for long-term predictions of significant wave height. *Coast. Eng.*, **51**(*5-6*): 387–394. https://doi.org/10.1016/j.coastaleng.2004.04.003

INFOPLAZA (2021). Waveclimate.com: The on-line offshore climate assessment system. URL http://waveclimate.com/cgi-bin/query

Inman, D.L., Bagnold, R. (1963). Littoral processes. The Sea, Vol. **3**: Ideas and Observations on Progress in the Study of the Seas: 529–553.

Jiang, A.W., Hughes, M., Cowell, P., Gordon, A., Savioli, J.C., Ranasinghe, R. (2011). A Hybrid Model of Swash-Zone Longshore Sediment Transport on Reflective Beaches. *Coast. Eng. Proc.*, **1**(*32*): p. sediment. 29. https://doi.org/10.9753/icce.v32.sediment.29

Kamphuis, J.W. (1991). Alongshore Sediment Transport Rate. *J. Waterw. Port, Coastal, Ocean Eng.*, **117**(*6*): 624–640. https://doi.org/10.1061/(ASCE)0733-950X(1991)117:6(624)

Komar, P. D. (1998). Beach processes and sedimentation. 2nd Edition, Prentice-Hall, Englewood-Cliffs, 544 p.

Kuriyama, Y., Sakamoto, H. (2014). Cross-shore distribution of long-term average longshore sediment transport rate on a sandy beach exposed to waves with various directionalities. *Coast. Eng.*, **86**: 27–35. https://doi.org/10.1016/J.COASTALENG.2014.01.009

Longuet-Higgins, M.S. (1970). Longshore currents generated by obliquely incident sea waves: 1. *J. Geophys. Res.*, **75**(*33*): 6778–6789. https://doi.org/10.1029/JC075i033p06778

Mackay, E.B.L., Challenor, P.G., Bahaj, A.B.S. (2010). On the use of discrete seasonal and directional models for the estimation of extreme wave conditions. *Ocean Eng.*, **37**(*5-6*): 425–442. https://doi.org/10.1016/j.oceaneng.2010.01.017

Mil-Homens, J., Ranasinghe, R., van Thiel de Vries, J.S.M., Stive, M.J.F. (2013). Re-evaluation and improvement of three commonly used bulk longshore sediment transport formulas. *Coast. Eng.*, **75**: 29–39. https://doi.org/10.1016/J.COASTALENG.2013.01.004

Munch-Peterson, J. (1938). Littoral drift formula. *Beach Erosion Board Bull.*, U.S. Army Engineer Waterways Experiment Station, Vicksburg, MS, **4**(*4*): 1–31.

Salcedo-Castro, J., Da Silva, N.P., De Camargo, R., Marone, E., Sepúlveda, H.H. (2018). Estimation of extreme wave height return periods from short-term interpolation of multi-mission satellite data: Application to the South Atlantic. *Ocean Sci.*, **14**(*4*): 911–921. https://doi.org/10.5194/OS-14-911-2018

Salem Cherif, Y., Mezouar, K., Guerfi, M., Sallaye, M., Dahmani, A.E.A. (2019). Nearshore hydrodynamics and sediment transport processes along the sandy coast of Boumerdes, Algeria. *Arab. J. Geosci.*, **12**(*24*): 1–17. https://doi.org/10.1007/s12517-019-4981-0

Sallaye, M., Mezouar, K., Dahmani, A., Cherif, Y.S. (2022). Coastal vulnerability assessment and identification of adaptation measures to climate change between Cape Matifou and Cape Djinet Algeria. *Geo-Eco-Marina*, **28**: 181–193. https://doi.org/10.5281/zenodo.7493268

Saville, T. (1950). Model study of sand transport along an infinitely long, straight beach. *Eos, Trans. Am. Geophys. Union*, **31**(*4*): 555–565. https://doi.org/10.1029/TR031I004P00555

Shaeri, S., Etemad-Shahidi, A., Tomlinson, R. (2020). Revisiting Longshore Sediment Transport Formulas. *J. Waterw. Port, Coastal, Ocean Eng.*, **146**(*4*), 04020009. https://doi.org/10.1061/(ASCE)WW.1943-5460.0000557

Shanas, P.R., Sanil Kumar, V. (2014). Coastal processes and longshore sediment transport along Kundapura coast, central west coast of India. *Geomorphology*, **214**: 436–451. https://doi.org/10.1016/J.GEOMORPH.2014.02.027

Tomasicchio, G.R., D'Alessandro, F., Barbaro, G. (2011). Composite modelling for large-scale experiments on wave-dune interactions. *J. Hydraul. Res.*, **49**(*sup1*): 15–19. https://doi.org/10.1080/00221686.2011.604576

Van Rijn, L. (1993). Principles of Sediment Transport in Rivers, Estuaries and Coastal Seas. *Aqua Publications*, Amsterdam, The Netherlands, URL https://www.worldcat.org/fr/title/29969144.

Van Rijn, L.C. (2014). A simple general expression for longshore transport of sand, gravel and shingle. *Coast. Eng.*, **90**: 23–39. https://doi.org/10.1016/J.COASTALENG.2014.04.008

Vinoth, J., Young, I.R. (2011). Global estimates of extreme wind speed and wave height. *J. Clim.*, **24**: 1647–1665. https://doi.org/10.1175/2010JCLI3680.1